Journal of King Saud University – Engineering Sciences (2025) 37:52
https://doi.org/10.1007/s44444-025-00044-4

ORIGINAL PAPER

Development of Multi-Objective Particle Swarm Optimisation (MOPSO) strategy in enhancing interference mitigation in Machine-to-Machine (M2M) communication based on fault clearance and communication delay in Smart Grid Networks

Ahmed Danasabe Suleiman[1] · Ababubakar Saddiq Mohammmed[2] · Bala Alhaji Salihu[2] · Michael David[2] · Abdullahi Ibrahim Mohammed[3] · Ephraim Michael[4]

Received: 28 May 2025 / Accepted: 20 August 2025

Abstract
The proliferation of connected devices has led to a paradigm shift in cellular standards, typified by the long-term evolution (LTE) standard. The fifth-generation (5G) standard supportsnumerouspromising mobile technologies, including Machine-to-Machine (M2M) and Device-to-Device (D2D) communication, which enable the communication of a large number of intelligent devices and ubiquitous devices. The deployment of M2M devices in the application of smart grid (SG), specifically in power systems, has introduced new compromising challenges in the areas of resource allocation and interference management. The 5G cellular network's qualityofservice (QoS) and performance deteriorate due to interference brought on by the reduced inter-cell distance and the smooth integration of heterogeneous devices.In this paper, an interference-aware multi-objective particle swarm optimisation(MOPSO)scheme is proposed for M2M communication in SG to mitigate the interference generated as a result of the localisation of M2M devices on the grid. In order to evaluate performance, the MOPSO approach was developed and implemented for smart grid situations based on pre-fault, during-fault, and post-optimisation conditions. The initial step was to use the multi-objective particle swarm optimisation (MOPSO) algorithm to optimise the smart grid network in order to decrease grid interference. According to simulation results, under different pre-fault and post-optimisation settings, the system throughput and signal-to-interference-to-noise ratio (SINR) were greatly increased by 32.69 and 21.94%, respectively. Furthermore, by using MOPSO, the fault clearance time was reduced by 106.06%, reducing the amount of time needed to clear an impending fault with interference. Additionally, the smart grid network's power loss was improved and maintained at levels comparable to those of the pre-fault conditions. In the subsequent step, the performance of the developed MOPSO technique was compared to that of the non-dominated sorting genetic algorithm (NSGA-II) in terms of convergence in fault clearance time, SINR, and throughput. Simulation results indicated that, in comparison to NSGA-II's performance, MOPSO throughput and SINR were enhanced by 5.93%, 4.65%, and 0.96%, respectively. In comparison to NSGA-II, the proposed MOPSO converges to the optimal solution more quickly for the various objective functions. The findings provided by the developed MOPSO demonstrate that it can efficiently compete with similar algorithms when tackling problems involving interference optimisation algorithms.

Keywords Machine-to-machine (M2M) · Smart grid (SG) · Multi-objective particle swarm optimisation (MOPSO) · Interference mitigation · Fault clearance time

1 Introduction

The increase in complexity and demand has put a great deal of strain on the modern energy landscape and conventional electrical power systems, due to some constraints, such as ineffective power distribution, fault monitoring, and detection, which have caused great inefficiency (Labrador Rivas and Abrão 2020). To address these problems, smart grids (SGs) have surfaced as a solution, combining distributed generation (DG) techniques, communication technologies, and sophisticated network monitoring (Achaal et al. 2024). They offer a two-way communication system that

Extended author information available on the last page of the article

Published online: 24 November 2025

makes it easier to automate processes, integrate renewable energy sources efficiently, and regulate them in real time. Centralised monitoring and data gathering depend heavily on essential technologies like smart meters and Phasor measurement units (PMUs), which are made possible by machine-to-machine (M2M) communication. These characteristics allow the delivery of reliable, sustainable, high-quality power to satisfy changing customer expectations in addition to improving operational efficiency. By enhancing the overall electrical network's efficiency, security, and adaptability, smart grid systems seek to completely transform the way energy is delivered (Saini et al. 2021). This is attained through facilitating real-time data sharing between several smart components, including meters, circuit breakers, and distributed energy sources. The integration of the internet of things (IoT) devices further improves smart grids. These devices use distributed computation and reliable bi-directional connectivity to help move from traditional power systems to dynamic smart grids. IoT enables smart grids to increase automation, better fault detection, and lower energy losses. A more robust and responsive grid that can efficiently handle decentralised and varied power inputs is promised by this combination of IoT and smart grid technologies (Antonius Alijoyo et al. 2024).

The complete realisation of smart grid capabilities depends on the deployment of the fifth-generation (5G) network. It is perfect for managing the rigorous demands of SG communications because of its high speed, low latency, and capacity to accommodate huge device connectivity (Shahinzadeh et al. 2021). Critical applications like teleprotection, which require packet loss of 10^{-9} and end-to-end latency of less than 5 ms response time to prevent equipment damage during perceived faults, depend on 5G's ability to transmit data quickly. Its ultra-low packet loss and large bandwidth capabilities guarantee steady operation and improve the dependability of systems such as wide area monitoring systems (WAMS). Additionally, 5G makes it easier to implement machine-type communication (MTC) and advanced metering infrastructure (AMI) services, establishing the foundation for future scalability and reliable energy management (Abdulkareem et al. 2021; Abdulsalam et al. 2023). Realising the full potential of smart grids requires the deployment of 5G technology (Majeed Butt et al. 2021). It is well-suited to satisfy the rigorous criteria of smart grid communications due to its high speed, low latency, and capacity to Support a large number of linked devices. The stringent specifications of IEC 61850-based smart grid environments, particularly concerning ultra-low latency, high reliability, and the capacity to support dense machine-type communication (MTC), motivated the selection of 5G as the communication backbone in this study. Although other technologies like Wi-Fi 6, ZigBee, LoRaWAN, and conventional LTE have advantages in terms of cost and deployment simplicity, they typically fall short of the ultra-low latency and quality of service (QoS) standards required for real-time Substation control and protection. However, deploying 5G comes with trade-offs, including higher infrastructure costs, increased integration complexity, and greater exposure to cybersecurity concerns due to its reliance on software-defined networking and edge computing. These highlight the competitive advantage of 5G adoption and preference over other alternative communication protocols (Patel et al. 2023).

Smart grid-enabled real-time monitoring is essential for enhancing fault identification and dependability, especially in geographically scattered distribution networks (Kabeyi and Olanrewaju 2023). Larger outages can be avoided with early discovery, as the majority of failures in these networks are temporary. Nonetheless, there are still issues because distribution lines are diverse, load patterns vary, and fault measurement capabilities are limited (Yasin Ghadi et al. 2024). Although advantageous, the incorporation of inverter-based microgrids adds another level of complexity. 5G's low latency and high dependability are essential for resolving these problems through data-driven monitoring and flexible device control (Suleiman et al. 2022). Furthermore, predictive maintenance, fault localisation, and an overall increase in grid resilience and operational intelligence are made possible by the deployment of IoT-enabled sensing devices and advanced analytics (Ullah et al. 2022).

A major change from centralised, one-way energy systems to decentralised, interactive, and self-healing networks is represented by the move to smart grids. By using data-driven technologies (DDTs) for fault management, energy trading, and load forecasting, smart grids seek to address issues that traditional grids suffer, such as high transmission losses and a lack of real-time control. Future grids must integrate cutting-edge communication systems that provide improved consumer involvement, fault tolerance, and monitoring in order to satisfy both technical and financial objectives. This transition entails addressing issues such as transmission line heat constraints and maintaining frequency and voltage stability. By integrating automatic generation control (AGC) systems, enhancing forecasting methods, employing energy storage, and building modern communication infrastructures, smart grids promise to supply secure, efficient, and sustainable power to both essential and general loads (Velasquez et al. 2024; Ahsan et al. 2023). This marks a significant shift in the design and administration of energy networks. However, to improve efficiency and reduce disruptions in the smart power system, fault analysis is crucial. To maintain the power system functioning normally, it is essential to identify, track down, and fix faults at any level (Labrador Rivas and Abrão 2020).

Communication network designs for smart grids require special consideration since they incorporate infrastructure elements such as control centres, grid stations, feeders,

substations, transformers, smart meters, and circuit breakers (Raza et al. 2019). Machine-to-machine (M2M) and smart grid devices are combined in the smart grid system to allow for monitoring and challenge management across a range of functions, including scheduling, demand-side management, demand response, unit commitment, network grid configuration, contingency planning, distributed generation allocation, transmission expansion, and generation expansion.

Smart grid development, which will include decentralised power generation, two-way energy trading, request coordination, and energy redistribution, is made possible by the deployment of cellular components (Hu et al. 2020). The smart grid's two-way communication and electric flow capabilities enable reliable automatic energy services to be delivered effectively and safely (Abdulkareem et al. 2021).

In smart grid (SG) setups that comply with IEC 61850, the proposed integration of multi-objective particle swarm optimisation (MOPSO) for interference mitigation shows encouraging gains in SINR, throughput, and communication efficiency. When integrating the power and communication domains in real-world systems, however, there are practical implementation issues that must be addressed. In order to achieve precise protection coordination, time-critical problem detection, and event analysis, intelligent electronic devices (IEDs) must first synchronise with one another. Time-stamped signals like sampled values (SV) and generic object-oriented substation event (GOOSE), which are crucial to IEC 61850-based communication, need to be timed precisely to guarantee consistency between devices (Nguyen et al. 2025). Protocols Such as IEEE 1588 precision time protocol (PTP) or Global Positioning System (GPS)-based synchronisation must be used to achieve sub-millisecond precision requirements. In the absence of this, asynchronous messaging could result in miscommunication between substations and control centres, resulting in delayed fault isolation or false tripping (Yamashita et al. 2022). In addition, the growing integration of Information Technology (IT) and Operational Technology (OT) systems in contemporary Substations presents a serious security concern. Since IEC 61850 messages—especially GOOSE and SV—are usually sent over ethernet and are not encrypted or authenticated by default, they are susceptible to denial-of-service (DoS) attacks, packet injection, and spoofing (Elrawy et al. 2023). These risks could be used to alter device behaviour or interfere with protection logic. Future integrations of the suggested system ought to include cybersecurity features based on IEC 62351, like role-based access control, secure key management, and digital signatures, in order to lessen this. To guarantee robustness, interference mitigation algorithms like MOPSO should also be tested in cyber attack scenarios. Furthermore, the time between the identification of a disturbance and the breaker action must be within 2 to 4 ms, making real-time responsiveness a crucial need in smart grid protection and control systems (Gaspar et al. 2023). Although MOPSO works well for multi-objective optimisation, these stringent time limitations must be considered when assessing its computational complexity. Although the current model is intended for low-latency execution, hardware-in-the-loop (HIL) simulation utilising platforms such as OPAL real-time technologies (OPAL-RT) or real-time digital simulator (RTDS) is necessary to validate its adoption in real-time protection systems (Wang et al. 2022). This verification will guarantee that the optimisation algorithm does not cause unforeseen delays that would jeopardise grid safety or stability. Furthermore, the integration of heterogeneous devices and the growing densification of M2M device networks across cellular systems face significant difficulties largely connected to managing interferences because of the reduction in inter-cell distances. The confluence of these elements makes it challenging to distribute resources and manage M2M communications interference, which lowers channel capacity and degrades primary user communication quality (Song et al. 2020). Co-channel interference (CCI) and adjacent channel interference (ACI) are two forms of interference that can be especially troublesome in 5G networks. In a multi-cell setting, the 5G network's densification and heterogeneity, as well as the shorter inter-cell distances, present architectural issues.

1.1 Key contribution of this paper

The key contribution of this paper is stated as follows:

i. We formulated the machine-to-machine (M2M) communication interference problem to attain maximised throughput and SINR while decreasing the interference. In this study, the intra-cell, inter-cell, and mutual interferences with constraints of transmit power, bandwidth, and separation distance were considered.
ii. We formulated the interference problem as a multi-objective particle swarm optimisation (MOPSO) and hence developed the MOPSO algorithm to solve the optimisation problem.
iii. We applied the developed MOPSO algorithm to minimise the fault clearance time, communication delay, and power loss within the context of a smart grid power system using the IEEE 9-bus system.
iv. Finally, we evaluated the performance of the algorithm and provide extensive simulation results to assess the performance of the MOPSO algorithm with varied fault conditions (pre-fault, during-fault, and post-optimisation).

The structure of the remainder of this paper is as follows: Section 2 discusses related works that underpin the fundamental concepts of interference. Section 3 discusses

the mathematical formulation of the interference problem and proposes the multi-objective particle swarm optimisation (MOPSO) scheme for interference mitigation. Section 4 presents the simulation results and analysis of the results, and finally, Section 5 concludes the paper.

2 Related works

Numerous approaches to managing interferences during machine-to-machine (M2M) communications in 5G networks have been published in the literature. Through spectrum allocation management, power control methods, and radio resource allocation, the tactics combat interferences. The interference problem that arises when using network flying platforms in ultra-dense tiny cells was investigated by AlSheyab et al. (2020). The study provides evidence of NP-hard problems with suboptimal solutions during its investigation of this issue. According to their concept, a bipartite machine and a local search-based algorithm are two suggested possibilities for reducing interference. A significant limitation of their study was the lack of investigation into interference among various system levels. The results of the simulation demonstrated effective interference reduction despite cross-tier interference being excluded from the study. Additionally, an optimal strategy for minimising interference to improve system throughput in cellular networks that serve M2M devices was presented by Dubey et al. (2020). Cell subdivision-based resource distribution, channel allocation, and dependable particle swarm optimisation for mid-cell power design are the three components that the system uses for power allocation. According to simulation data, network performance is increased by better interference reduction techniques; however, network throughput sharply drops as soon as M2M devices go beyond a certain threshold. The study solely considered co-channel and cross-channel interference, while the influence of mutual interference was not considered.

HAPPIER, a learning-based interference management system for UAV-mounted small cells, was presented by the authors Cheng et al. (2021). In order to manage co-channel interferences, the HAPPIER system employs power control schemes for aerial small cells (ASCs). To maximise transmit power and speed up learning processes, the system combines reinforcement learning with hybrid affinity propagation clustering. Their system achieves 93% of the maximum throughput that would be possible with exhaustive search techniques when it modifies the gearbox power levels. This study ignored both co-channel and mutual interference when calculating interference and only addressed cross-interference issues in M2M communications. According to Kumar et al. (2021), the signal-to-interference plus noise ratio (SINR) suffers as power transmission from eNodeB devices decreases in tandem with increasing throughput needs. The study shows that SINR performance improves with increasing throughput, but it ignores all interferences caused by different cell environments. For public safety and ubiquitous network applications, the authors (Barman and Ajay 2020) created a collaborative approach for resource allocation, communication mode selection, and interference cancellation in M2M communication using licensed cellular bands. The authors reduced spectrum interference between frequency-overlapping cells and improved minimum mode selection by using power-based management in conjunction with orthogonal precoding. According to simulation results, the suggested orthogonal precoding method performed better than traditional precoding techniques when used in highly interfered locations. Interferences between nodes in the same tier and between nodes in separate tiers were not resolved by the procedure. By integrating power control and mode selection under power and SINR limits in interference-limited zones, Liu et al. (2020) presented PC-ILA as a method to improve system data rates. In addition to optimising coverage probability and mode selection in high-SINR situations, the method offers better sum data rates than current approaches when traffic density rises.

Osama et al. (2021) proposed a Soft Frequency Reuse technique to minimise the impact of interference and improve power efficiency simultaneously by applying on/off switching to the interference contribution rate. According to this method, the system-wide data rate increases when the optimal centre radius zones are identified. When more eNodeBs and fewer M2M devices were not included in the experiment, the power consumption was at its lowest. Co-tier interference between devices that share a common network was the sole focus of the study. For machine-type devices (MTDs) operating in constrained spectrum, Wang et al. (2021) created a mechanism for allocating spectrum and power utilisation. This method performs spectrum allocation through the iterative channel allocation and power control mechanism with a non-aggressive approach. By allocating spectrum resources to MTDs, the algorithm lowers interference levels. Nevertheless, it is 0.5% less than the optimal signal-to-interference-plus-noise ratio (SINR) that Monte Carlo simulations may achieve.

For cellular network M2M communications, Das and Hossain (2020) created a location-based power controller that decreases interference and increases energy and spectrum efficiency through a combination of water-filling optimisation together with a Lagrange decomposition framework. Determining the optimal M2M pair distances for the best data rates was the limitation of the study. Similarly, the location-based technique developed by Hassan and Fernando (2019) uses system loading levels, user mobility patterns, traffic variations, and signal-to-interference-plus-noise ratio measurements to handle base station network interference. Unbalanced loads and failure to account

for interference between M2M-eNodeB interactions and machine-to-machine connections are some of its drawbacks. Pourkabirian et al. (2021) in their study limited the influence of interference by optimising the transmit power in 5G femtocell networks using a game-theoretic method. Using learning principles, a user-specific optimisation approach assisted in determining the optimal transmission power levels while taking interference and QoS constraints into account. Improved operating performance and service quality, together with fewer disturbances to nearby systems, were captured by the simulation.

There are many different ways to reduce interference in Smart Grid communication, especially in M2M and IEC 61850-based systems. Conventional metaheuristic algorithms have shown satisfactory performance under controlled or static network settings, including standard particle swarm optimisation (PSO), genetic algorithms (GA) (Shafiei et al. 2021), and ant colony optimisation (ACO) (Alam et al. 2024). The dynamic topologies and high device densities that define contemporary 5G-enabled smart grids, however, frequently make it difficult for these methods to adapt in real-time scenarios. The difficulty lies in optimising and balancing competing objectives, such as maximising SINR and system throughput, while minimising interference, power consumption, and delay. However, being trapped in local optima and slow convergence speeds are common drawbacks associated with some of these techniques. Furthermore, signal-level coordination schemes work well in isolated situations (Hao et al. 2023; Su et al. 2025), but they are frequently centralised and therefore are not scalable or resilient to communication failures or node mobility. Additionally, many of the current methods optimise a single objective (such as throughput or delay), ignoring the intricate trade-offs that are present in multi-objective smart grid environments.

On the other hand, our suggested multi-objective particle swarm optimisation (MOPSO) scheme is specifically made to fill in these gaps by allowing the simultaneous optimisation of several goals, most notably SINR and total network throughput, while contending with limitations like power limits, distance thresholds, and real-time latency requirements. In order to prevent premature convergence, the MOPSO variation utilised here maintains diversity in the Pareto front by utilising crowding distance sorting and adaptive inertia weights. In addition, numerous research approaches suggest that the interference mitigation techniques proposed by several studies have not comprehensively addressed the challenging compromise of managing cross-tier interference, co-tier interference, and mutual interference simultaneously. However, in this study, the problem of interference in machine-to-machine (M2M) communication underlaid in 5G networks with applications in smart grids has been investigated. Furthermore, obtaining an optimal solution is difficult since optimising interference involves navigating trade-offs between numerous objectives with different limitations, which is complicated by the nature of the objective functions. To justify improving throughput and signal-to-interference-plus-noise ratio (SINR) within the communication domain, and also maximising the communication delay time, fault clearance time, and power loss within the smart grid system, this study employs a multi-objective particle swarm optimisation (MOPSO) approach to resolve the optimisation complexity within the communication and power domain.

3 Methodology

3.1 System model

In this paper, the system model represents an integration of the IEEE 9-bus power system with a network of 5G communication architecture, where M2M devices underlaid in 5G coexist with CUEs across a multi-cell environment. This scheme focuses on the minimisation of interference (fault clearance) resulting from the communication of MTDs within the power system. A centralised interference-aware architecture is considered where the radio resource is assigned by the eNodeB, as depicted in Fig. 1 below.

From Fig. 1 shown above, it is assumed that the M2M transmitter has its designated M2M receiver located within the coverage area of transmission, and the M2M transmitter can communicate directly with the M2M receiver without the influence of the eNodeB. This proximity communication, which is characterised by low-power M2M links, coexists with CUEs. The channel state information (CSI) of the CUEs in the uplink is estimated by the eNodeB, while the CSI of the M2M links is estimated by the M2Ms, and then the report is fed back to the eNodeB via the uplink idle band for transmission. It is assumed that eNodeBs within the same cell share the same frequency band, thereby resulting in intra-channel interference, while eNodeBs in adjacent cells that share the same frequency band with CUEs in other cells cause inter-cell interference. The connectivity to an eNodeB by uniformly distributed CUEs is based on the association proximity to where their maximum power is received in the uplink. The machine-type-devices (MTDs) embedded into the power grid are utilised to detect and monitor faults resulting from interference experienced within the grid. The subchannel resources are assumed to be occupied at most by one CUE and one M2M in the uplink direction. The resultant system bandwidth W of the CUEs is shared into a B number of subchannels, and each M2M uplink utilises a single subchannel which is dynamically assigned. The set of index for the subchannels is given as $B = \{1, 2, 3, 4, ...b\}$, the subchannel bandwidth of each is given as $W_0 = \frac{W}{B}$ and with the assumption that

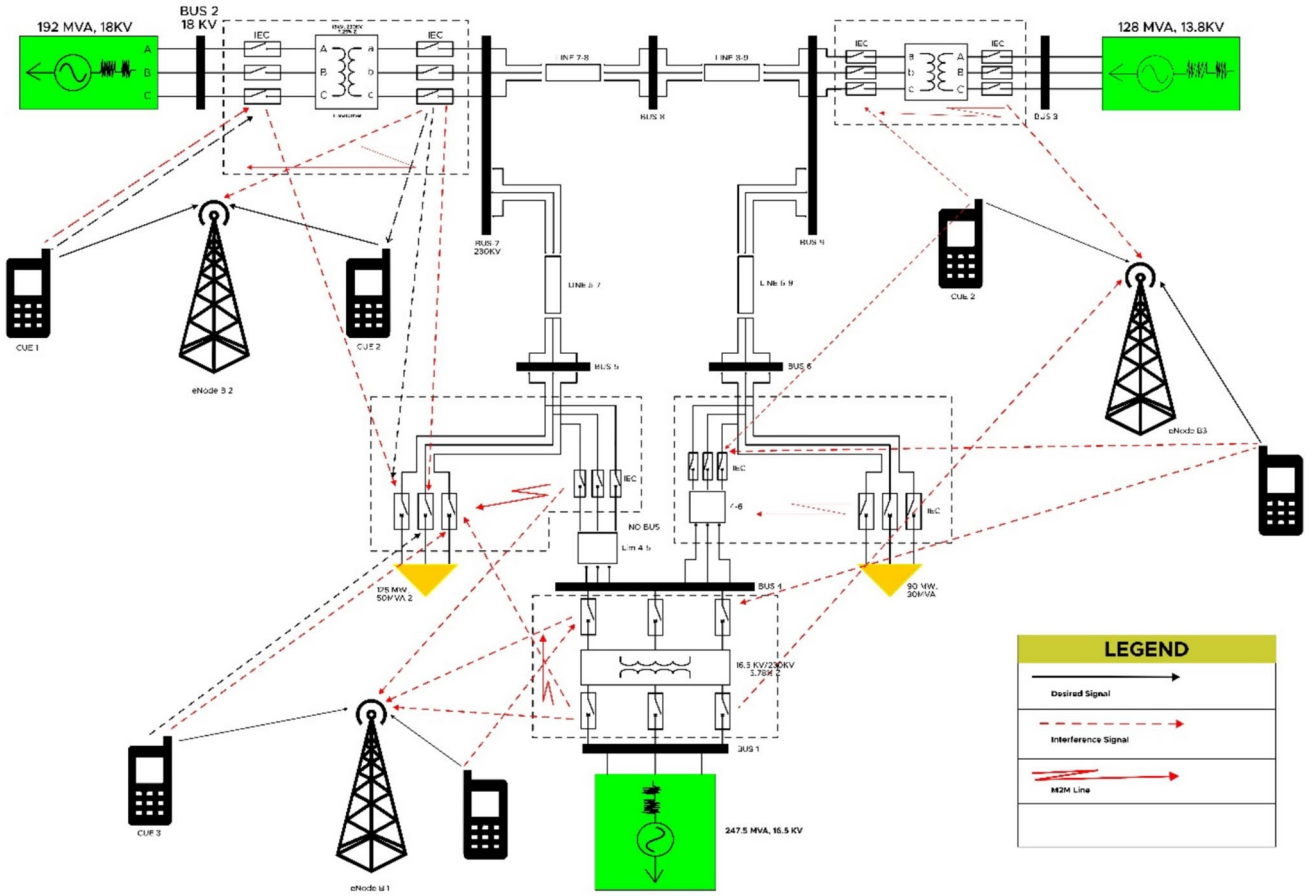

Fig. 1 System model depicting the M2M interference scenarios with the smart grid network

their K CUEs and V MTDs have their uplink links index set as $U^K = \{1, 2, 3, 4, ...k\}$ and $U^V = \{1, 2, 3, 4, ..., v\}$, respectively. Furthermore, the M2M transmitters ($M2M_{TX}$) are randomly distributed within the smart power grid, and also the M2M receivers ($M2M_{RX}$) are equally distributed within the confines of their predetermined transmitter with a separation distance d.

3.2 Problem formulation

The interference problem between CUEs and MTDs within the network of a smart power grid is influenced by some pivotal constraints: the separation distance between M2M, transmission power, and the bandwidth allocation by each MTD. This study aims to minimise the impact of interference in a smart grid power system while maximising the following communication metrics, such as signal-to-interference-plus-noise ratio (SINR) and the overall system throughput. In the power grid, metrics such as the fault clearance time, delay communication time, and power loss are enhanced. The sum of interference is considered between CUEs and M2M pairs, M2M pairs and another M2M pair, and mutual interference between the $M2M_{TX}$ and $M2M_{RX}$.

We assume an imperfect channel state model (CSI), where the actual gain is the summation of the estimated gain and the estimated error, which is denoted by Eq. (1).

$$e = (\overline{e}^{C_n} + \overline{e}^{M_n}) + \Delta(e^{C_n} + e^{M_n}) \tag{1}$$

where e is the actual channel vector, $\overline{e}^{C_n}, \overline{e}^{M_n}$ represents the estimated channel vector for both the CUEs and M2M devices respectively, and $\Delta e^{C_n}, \Delta e^{M_n}$ is the estimated error vector for both the CUEs and M2M devices respectively, which is usually assumed to be $\Delta e^{C_n} \sim C\aleph\left(0, \sigma^2_{C_n} I\right)$ and $\Delta e^{M_n} \sim C\aleph\left(0, \sigma^2_{M_n} I\right)$ a complex Gaussian noise with zero mean and variance σ^2_e. But for the CUEs, the actual channel model from the CUEs to the eNodeB can also be stated as follows:

$$e^{C_n} = \overline{e}^{C_n} + \Delta e^{C_n} \tag{2}$$

$$e^{M_n} = \overline{e}^{M_n} + \Delta e^{M_n} \tag{3}$$

This can also be rewritten for the CUEs in the scalar form as $e^{C_n} = \overline{e}^{C_n} + \partial e^{C_n}, \partial e^{C_n} \sim C\aleph\left(0, \sigma^2_{C_n}\right)$ and $e^{M_n} = \overline{e}^{M_n} + \partial e^{M_n}, \partial e^{M_n} \sim C\aleph\left(0, \sigma^2_{M_n}\right)$. With the assumption that the channel errors are small $\left(\partial \ll \overline{e}\right)$, the squared channel gain can be expressed as follows:

$$|e|^2 = \left|\overline{e} + \delta\right|^2 = \left|\overline{e}\right|^2 + 2\Re\left\{\overline{e} * \delta\right\} + |\delta|^2 \tag{4}$$

Taking the expectation

$$\mathrm{E}\left[|e|^2\right] = \left|\overline{e}\right|^2 + \sigma^2_{\delta} \tag{5}$$

It was assumed that an M2M pair can meet the QoS requirements of the entire communication system with minimal power consumption by reusing multiple channel resources to assure packet transmission success. Furthermore, the CUE's signal-to-interference-plus-noise-ratio (SINR) can be written as $\xi_j^{C_n}$. The SINR must be higher than ξ^* for transmission to be successful. Where ξ^* the threshold for different M2M devices is placed within the power grid.

Therefore,

$$\mathrm{E}\left[\xi_j^{C_n}\right] > \xi^*, \quad \forall j \in N \tag{6}$$

For the *nth* M2M link on the j th channel, the expected SINR is expressed by the following:

$$\mathrm{E}\left[\xi_j^{M_n}\right] = \frac{P_j^{M_n}\left(\left|\overline{e_j^{M_n}}\right|^2 + \sigma_j^2\right)}{P_j^{C_m}\left(\left|\overline{e_j^{C_m}}\right|^2 + \sigma_j^2\right) + \sum_{h=1,h\neq n}^{N} P_j^{M_h}\left(\left|\overline{e_j^{M_h}}\right|^2 + \sigma_j^2\right) + N_a + \sigma^2} \tag{7}$$

where $P_j^{M_n}$ is the transmit power on the M2M link on the j th channel and $\overline{e_j^{M_n}}$ denotes the estimated channel gain between the M2M-Tx and M2M-Rx, respectively. Moreso, $P_j^{C_m}$ on the j th channel represents the transmit power by the m th CUE and $P_j^{M_h}$ denotes the transmit power of the h th M2M link. The estimated link gain of the m th CUE and h th M2M link on the j th channel is denoted by $\overline{e_j^{C_m}}$ and $\overline{e_j^{M_h}}$, respectively. The additive white Gaussian noise (AWGN) power is given as σ^2, N_a represents the average interference (noise) emanating from other surrounding neighbouring cells, which can be expressed as below. Similarly, the SINR of the m th CUE on the j th channel can be denoted as follows:

$$\mathrm{E}\left[\xi_j^{C_n}\right] = \frac{P_j^{C_m}\left(\left|\overline{e_j^{C_m}}\right|^2 + \sigma_j^2\right)}{\sum_{i=1}^{K}\sum_{y=1,}^{N} P_i^{M_y}\left(\left|\overline{e_i^{M_y}}\right|^2 + \sigma_i^2\right) + N_a + \sigma^2} \tag{8}$$

where the transmit power of the m th CUE and the transmit power of the y th M2M link the reusing the i th channel, are given as $P_j^{C_m}$ and $P_i^{M_y}$ respectively, while the channel gain of the m th CUE and the channel gain of the y th M2M link, reusing the i th channel is denoted as $\overline{e_j^{C_m}}$ and $\overline{e_i^{M_y}}$, respectively, as shown in Eq. (3).

$$N = E \cdot \sum P_w \cdot S_w^{-\alpha} \forall w \in \{1, 2, 3, ...W\} \tag{9}$$

where S is the sum of Euclidean distance between two M2M pairs and CUE, w represents the number of neighbouring cells, and E is the link gain. However, the distance between the CUEs and the M2M pair can be expanded and represented relative to the coordinates of the various devices. Considering $(s_{i,b}, s_{j,b})$ and $(S\,S_{j_{1_1},b}, s_{j_1,b})$ as the coordinates of the positions of the M2M pairs and a cellular user, then the distances is the Euclidean distance between two M2M pairs $s_{j,j}$ and the cellular $s_{i,j}$ is given as (Kaufman et al. 2013)

$$s_{j,j} \leq \left(\frac{s_{i,j}^{\alpha}(\Omega - 1)s_{j,b}^{\alpha} e_{j,j} e_{i,b}\left(\overline{e_{j,b}}\right)^{-1}}{\xi_j^m e_{j,j}\left[\Omega\xi_i^{c,b} s_{i,b}^{\alpha} e_{i,j} + s_{i,j}^{\alpha} e_{i,b}\right]}\right)^{\frac{1}{\alpha}} \triangleq s_{\max} \tag{10}$$

where $s_{\max}$ signifies the maximum transmission distance of the M2M source. This further defines the location of the destination where the M2M receiver must be localised to attain the required minimum SINR $\xi^m_{j,\min}$ of the M2M. The distance between the CUE and the M2M devices, the distance between the M2M-TX and eNodeB, and the distance CUE and eNodeB are represented as $s_{i,j}^{\alpha}$, $s_{j,b}^{\alpha}$, and $s_{i,b}^{\alpha}$ respectively. Furthermore, $e_{j,j}$, $e_{i,b}$, $e_{i,j}$, and $\overline{e_{j,b}}$ denotes the gain between the M2M-Tx and M2M-RX, CUEs and eNodeB, and CUEs and M2M devices, and the estimated gain between the M2M devices and eNodeB, respectively. Where Ω represents the scaling factor. In order to satisfy the SINR constraint by an M2M link and not being in outage, the link probability is given as $Pr\left[S_{max} \geq S_{j,j}\right]$. The overall system capacity of a given cell is expressed as follows (Pandey and Arya 2022):

$$\max_{\omega_{i,j},P_j^m} R_{overall} = \sum_{b\in N_s}\sum_{i\in P}\left[W(\log_2(1+\xi_j^{C_n}) + \sum_{j\in Q}\omega_{i,j}\log_2(1+\xi_j^{M_n}))\right] \tag{11}$$

where W represents the bandwidth.

$$\max_{\left\{\omega_{i,j},P^{N_{i,b}},P^{m_j},z_k^j,w_k^j\right\}} R_{overall} = \sum_{k=1}^{k}\sum_{i=1}^{C} w_i^k C_i^{c_i,b}(p_k^{c_i,b},p_k^{m_j}) + \sum_{k=1}^{k}\sum_{j=1}^{M} z_j^k C_k^{m_j}(p_k^{c_i,b},p_k^{m_j}) \tag{12}$$

$$subject\ to: \quad \sum_{k=1}^{K} w_i^k = 1, \qquad \forall i \in C,\ w_i^k \in \{0,1\} \tag{13}$$

$$\sum_{k=1}^{K} z_j^k \leq, \qquad \forall j \in M,\ z_j^k \in \{0,1\} \tag{14}$$

$$\sum_{k=1}^{C} w_i^k = 1, \qquad \forall k \in K,\ w_i^k \in \{0,1\} \tag{15}$$

$$\sum_{k=1}^{D} z_j^k \leq, \qquad \forall k \in K,\ z_j^k \in \{0,1\} \tag{16}$$

Using the spectrum allocation variable w_i^k,z_j^k and power allocation variables $p_k^{c_i}$,$p_k^{m_j}$, the objective function of Eq. (12) seeks to maximise the system's overall network throughput in a way that does not compromise the M2M and cellular networks' QoS requirements. Each CUE i and M2M pair j can only access one RB, and the M2M pair can only exploit one RB at most, as indicated by constraints Eqs. (13) and (14). Additionally, each RB can be assigned to a maximum of one M2M connection and one cellular link, respectively, according to constraints Eqs. (15) and (16).

$$\max_{\omega_{i,j},P_j^m} R_{overall} = \sum_{b\in N_s}\sum_{i\in P}\left[\log_2(1+\vartheta_i^{c,b}) + \sum_{j\in Q}\omega_{i,j}\log_2(1+\vartheta_j^m)\right] \tag{17}$$

$$subject\ to:$$

$$\vartheta_i^{c,b} = \frac{P_i^{c,b} r_{i,b}}{\sum_{j\in M}\omega_{i,j}P_j^m I_{j,b} + \sigma_N^2} \geq \vartheta_{i,\min}^{c,b}, \qquad \forall i \in C, \forall b \in N_s \tag{18}$$

$$\vartheta_j^m = \frac{P_j^m r_{j,j}}{\sum_{B\in N_s}\sum_{i\in C}\omega_{i,j}P_j^{c,B} I_{i,j}^B + \sigma_N^2} \geq \vartheta_{j,\min}^m, \qquad \forall j \in M, \tag{19}$$

$$\omega_{i,j} \in \{0,1\}, \qquad \forall i \in C,\ \forall j \in M, \tag{20}$$

$$\sum_i \omega_{i,j} \leq 1,\ \omega_{i,j} \in \{0,1\}, \qquad \forall j \in M \tag{21}$$

$$\sum_j \omega_{i,j} \leq 1,\ \omega_{i,j} \in \{0,1\}, \qquad \forall i \in C \tag{22}$$

$$0 \leq P_i^{c,b} \leq P_{mac}^{c,b} \qquad \forall i \in C \tag{23}$$

$$0 \leq P_j^m \leq P_{max}^m \qquad \forall j \in M \tag{24}$$

Similarly, $\omega_{i,j}$ is the channel reuse factor indicator for CUE i and M2M pair j, when M2M pair, j reuses the CUE i, $\omega_{i,j} = 1$; else $\omega_{i,j} = 0$ from Eq. (17). Constraints Eqs. (18) and (19) respectively represent the QoS requirements of the M2M pair and CUEs. Constraint Eq. (20) represents the interaction between CUEs i and M2M, j representing the channel reuse in conjunction with the resource sharing model. Moreover, constraint Eq. (21) demonstrates that a maximum of one M2M pair can share the CUE's RB. However, in the scenario where the M2M pair shares no more than one existing CUE's RB, as shown in constraint Eq. (22). Every restriction is used to lessen the complicated interference environment that M2M communications have produced. Nevertheless, the power budget of both MTDs and CUEs is limited to a maximum value by restrictions Eqs. (23) and (24). The combinatorial and non-convex optimisation problem can be reduced to a three-dimensional matching problem, which is known to be non-deterministic polynomial (NP)-hard. This complexity arises from the challenges of joint spectrum splitting and power management. However, by using a comprehensive and iterative approach, it is possible to find the best feasible solution by systematically examining all potential options w_i^k,z_j^k, and $p_k^{c_i}$,$p_k^{m_j}$. The formulated approach utilises a binary variable to represent the resource allocation decision, indicating which M2M pair can share the same spectrum resource with the CUE. Additionally, a continuous variable represents the power control strategy, reflecting the amount of transmission power designated for the potential M2M transmitter. Due to the complexity and non-linearity of the objective function, it results in a combinatorial optimisation problem, which limits the capacity of classical optimisation techniques to find unique solutions based on the high multi-dimensionality of the objective function.

3.3 The proposed multi-objective particle swarm optimisation (MOPSO) technique

The popular population-based metaheuristic method known as particle swarm optimisation was motivated by the social behaviour of particles, such as the movement of fish or birds. The primary parameters in this algorithm are each particle's position and velocity. Based on its own experiences and those of its neighbouring particles, each particle modifies its position inside the multidimensional search space. Local and global search techniques are combined in the PSO approach (Yuan et al. 2023). The particle's initial position is chosen at random to begin the PSO algorithm's initialisation; after which the objective function is used to determine the fitness

value. In every iteration, every particle moves closer to the two optimal values, Pbest and Gbest. Gbest is the population's best solution, while Pbest is the best solution each particle has produced. In this paper, after interacting with the surroundings, the M2M transmitter learns an effective joint channel splitting and selection with a power control policy. Generally speaking, when more M2M users utilise the cellular channels, the transmission power of M2M users increases, and cellular users experience increased interference. Our methodology maximises SINR and system ergodic capacity (throughput) while satisfying service expectations by allowing each M2M pair to adaptively optimise and trade off multi-objective particle (channel bandwidth, the optimal M2M separation distance, and power control methods). On the other hand, the algorithm also minimises the power loss and fault clearance time within the smart grid network, thereby ensuring reliability, improving grid resilience, and bringing about a reduction in downtime.

Using multi-objective particle swarm optimisation (MOPSO) technique can help tackle the aforementioned challenge, which is a complex multi-objective dilemma. The swarm particles are initialised based on the criteria that each particle (X) is an optimisable parameter for multi-objective problems. The particle symbolises the potential solution for distance, channel bandwidth, and power transmission. However, the velocity and positions of the particle are randomly initialised, as shown in Table 1.

Table 1 MOPSO optimisation parameters

Parameters	Values
Number of particles	50
Population size	500
Number of iterations	50
Inertia weight	0.9
Cognitive and social parameters	0.2
Archive size	100
Objective function	SINR and throughput
Optimisation constraints	Power, bandwidth, and distance

3.3.1 Particle initialisation

$$X = [\text{Power},\ \text{Bandwidth},\ \text{Distance}] \tag{25}$$

Each of the particles is expressed as a vector, and with several particle populations can be given as follows (Yuan et al. 2023):

$$X_{i,j} = [\text{PW}_{i,j}, \text{BW}_{i,j}, \text{DS}_{i,j}] \tag{26}$$

$$X_{i,j} = \begin{bmatrix} P\text{W}_{i,j}^{n} \\ B\text{W}_{i,j}^{n} \\ DS_{i,j}^{n} \end{bmatrix} \tag{27}$$

where PWi,j(n) is the power parameter PW for the n-th sample at position (i,j), BWi,j(n) is the bandwidth parameter BW for the n-th sample at position (i,j), and **DS**i,j(n) is the distance parameter DS for the n-th sample at position (i,j).

3.3.2 Fitness evaluation

The interference mitigation scheme is designed to optimise the crucial objective functions that significantly contribute to the influence of interference when underlaid in a 5G network. Hence, the resultant interference from the integration of M2M devices to the primary users' CUEs, thereby obtaining the effective spectrum allocation within the optimal separation distance and the optimal power allocation. The objective function utilised in this study can be expressed as.

i. Maximise the SINR to ensure the quality of communication is of high fidelity.
ii. Maximise the system throughput for efficient transmission of information.

Therefore, the maximisation of the sum of SINR and the overall system throughput can be expressed as follows:

$$\text{maximize}\left(F\left(X_{i,j}\right)\right) = [\text{SINR}, \text{Th}_{\text{overall}}] \tag{28}$$

subject to:

$$PW_{\min} \le PW_i \le PW_{\max},\ BW_{\min} \le BW_i \le BW_{\max}\ DS_{\min} \le DS_i \le DS_{\max}$$

where $\text{PW}_{\min}$ and $\text{PW}_{\max}$ represent the minimum and maximum transmission power limits, $\text{BW}_{\min}$ and $\text{BW}_{\max}$ denotes the minimum and maximum bandwidth limits, and $\text{DS}_{\min}$ and $\text{DS}_{\max}$ are the minimum and maximum distance limits.

3.3.3 Velocity and position update

For each of the particles (X), the velocity and position are regularly updated using the standard PSO equation. Each particle in the network updates its position and velocity based on its current position, personal best, and global best. The rule governing the velocity update is given by Eq. (30).

$$v_i^{(t+1)} = wv_i^{(t)} + c_1 r_1 (p_i^{(t)} - x_i^{(t)}) + c_2 r_2 (g^{(t)} - x_i^{(t)}) \tag{29}$$

where $v_i^{(t)}$ is the velocity of the particle, i at time t, w is the inertia weight (controls the exploration vs. exploitation trade-off), c_1 and c_2 are cognitive and social acceleration

coefficients, respectively. It is via the modification of c_1 and c_2 that the MOPSO could attain the required trade-off between cognitive and social behavioural patterns, r_1 and r_2 are random numbers uniformly distributed between 0 and 1, $p_i^{(t)}$ is the personal best position of the particle i, and $g^{(t)}$ is the global best position that has been explored by all the particles across the swarm. The particle's position is updated as follows:

$$x_i^{(t+1)} = x_i^{(t)} + v_i^{(t+1)} \tag{30}$$

3.3.4 Non-dominated sorting and Pareto front update

The programme then assesses the values of the objective function and updates the Pareto front after the particles have updated their positions and velocities. For multi-objective optimisation, the non-dominated sorting technique is used to find the solutions that no other solution dominates in both objectives (Pareto-optimal solutions). A solution x_i dominates another solution x_j based on the following condition:

If and only if:

1. $\text{SINR}_i \geq \text{SINR}_j$ and $\text{Throughput}_i \geq \text{Throughput}_j$.
2. At least one inequality is strict.

3.3.5 Archive update

Several non-dominated solutions that satisfy the Pareto optimality requirement are stored in the archive. As soon as the best new solutions are found, the archive is updated.

3.3.6 Convergence check

If the Pareto front is met or the predetermined number of iterations is reached, convergence is achieved; if not, the algorithm reverts to updating the velocity and position. The algorithm ends when it has converged, and the resulting solution yields a series of Pareto-optimal solutions, each of which represents the trade-off between maximising SINR and throughput. Therefore, the chosen network needs determines the ultimate choice. The suggested MOPSO scheme's flow chart is displayed in Fig. 2.

4 Performance evaluation

However, based on the IEEE 9-bus architecture, the communication structure of the smart grid, along with the machine-type devices (MTDs) and conventional power system devices, was incorporated. The IEEE 9-bus system consisted of a communication interface enabling data transfer between nodes within the grid, power generators, intelligent electronic devices (IEDs), transmission lines modelled with line constraints and impedance, and loads. The experiment and simulation were carried out using MATPOWER and MATLAB Simulink. The MOPSO algorithm, which was developed, was incorporated into the smart grid network's control layer. Its goal was to minimise fault clearance time and system power losses while simultaneously optimising and maximising SINR and system throughput. The practical limitations of transmission line capacity, voltage limitations, frequency limitations, and communication delays were considered during the simulation. To simulate different network conditions, such as pre-fault system conditions (when the grid system operates with a steady current and voltage profile), during-fault system conditions (when the system was simulated with a fault introduced as either a line-to-line or line-to-ground fault within a selected branch), and post-optimisation load conditions (when the system's control and reconfiguration actions were restored based on the integration of the MOPSO algorithm), simulations were carried out for varying numbers of M2M device deployments within a predetermined number of iterations. By simulating the load flow analysis during an interference and optimising the fault clearing time, this condition enhances the grid's ideal throughput and SINR. Throughout the simulation, numerous iterations were carried out, ranging from a minimum of 10 iterations to 50 iterations. Each generator, branch, and load bus's active power, reactive power, and voltage input characteristics were analysed under different circumstances (pre-fault, during-fault, and post-optimisation conditions). Tables 1, 2, 3, 4, 5, 6, and 7 illustrates the simulation parameters for the MOPSO optimisation, communication system, and IEEE 9-bus operating parameters for pre-fault conditions, power flow conditions for the pre-fault state, bus data and branch data parameters for the pre-fault conditions respectively.

The results of simulations conducted over the simulated smart grid network are displayed in Table 8. The optimisation goal was to maximise the SINR and throughput under two pre-defined network conditions (pre-fault and post-optimisation conditions) while reducing the communication delay time and fault clearance time under varying numbers of connected devices, ranging from 10 to 50 devices. Important findings from the simulations show that the algorithm greatly increased the SINR, particularly for 10 devices, from 37.00 to 64 dB (a 32-dB improvement). However, as Fig. 3 illustrates, the gain decreases with increasing device counts. Increased interference and a decrease in inter-cell distance are the reasons for the SINR gain's decline as the number of devices increases. Additionally, as illustrated in Fig. 4, the throughput of all the devices increased significantly. For example, the throughput of the 10-device count increased by 49.6%, indicating effective spectrum utilisation and being essential for real-time data transmission scenarios in smart

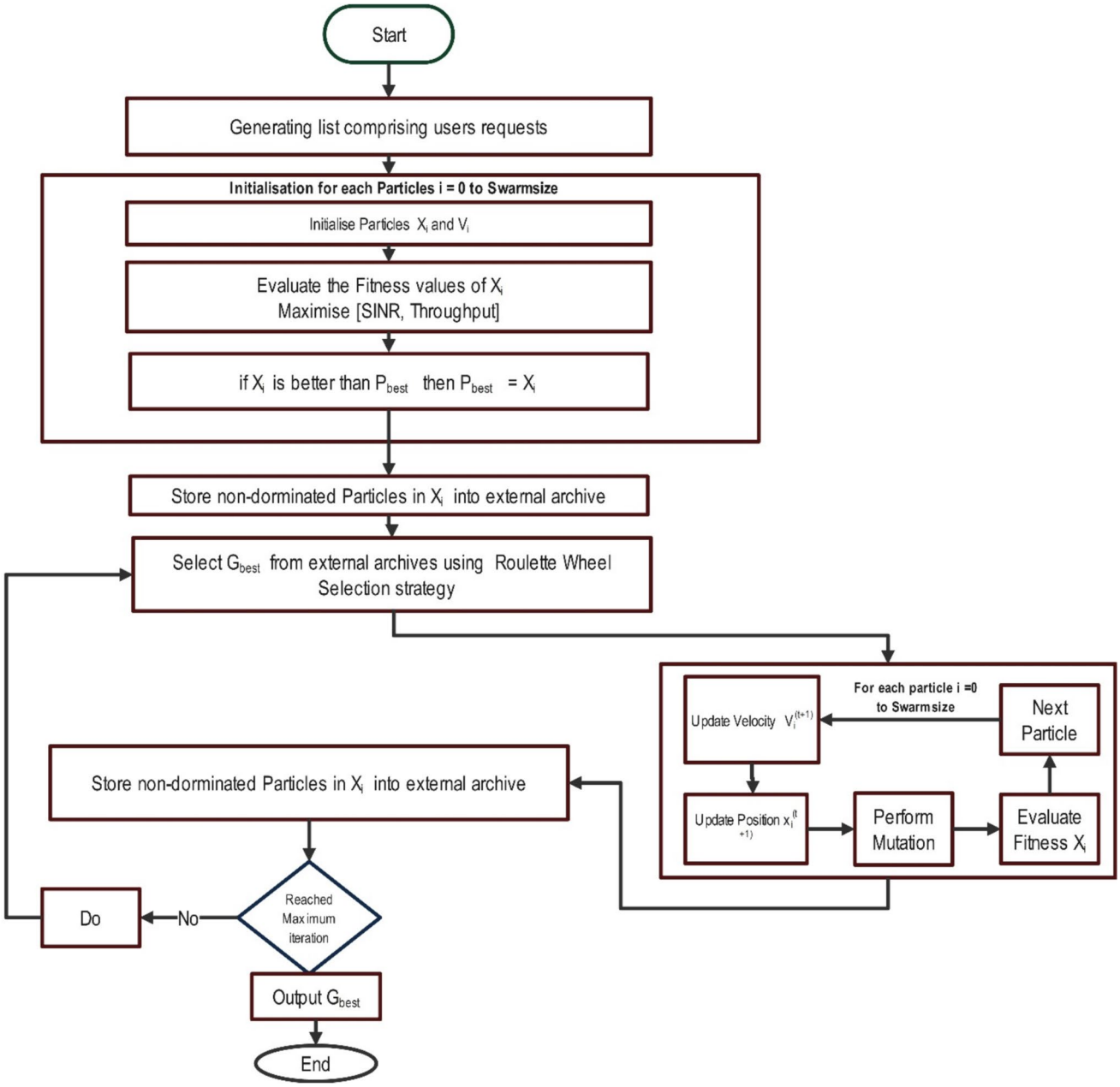

Fig. 2 The flow chart of the multi-objective particle swarm optimisation (MOPSO) (Suleiman et al. 2024)

grids. As a result, as shown in Fig. 5, the fault clearance time increased from 11.5 to 19.2%, improving the system power-protection responsiveness and guaranteeing quicker grid recovery. Additionally, all device counts indicated a decrease in delay time; for the lowest device count, the delay time was 66 ms before the pre-fault condition and 53 ms following the post-optimisation fault condition, indicating a 13 ms time lag.

According to the technical implications of Table 7, the improvement in SINR and reduction in system delay time indicate quick packet delivery with data reliability certainty, which is crucial for both control and protective devices like IEC 61850 GOOSE. Additionally, given the system's enhanced throughput, more devices can share the spectrum with CUEs without significantly degrading the channel. Figure 6 demonstrates how the smart grid network's resilience is increased as a result of faster communication and less damage in emergency scenarios (interference) due to its reduced communication delay time and rapid fault reaction. The simulation results also Suggest that a decrease in performance metrics is caused by rising device density, which is mostly due to increased interference and contention. The

Table 2 NSGA-II optimisation parameters

Parameters	Values
Population size	40
Generations	40
Crossover type	50
Crossover probability	0.8
Mutation type	Gaussian mutation
Mutation probability	0.1
Selection	Tournament
Objective functions	SINR and throughput
Constraints	Power, bandwidth, and distance

Table 3 Simulation parameters

Parameters	Values
eNodeB coverage radius (R)	500 m
Number of CUEs (L)	4
Number of M2Ms (K)	10, 20, 30, 40, 50
Subchannel bandwidth (B_0)	0.3215 MHz
Pathloss factor (a)	4
Noise power spectral density (N_0)	4×10–20 W/Hz
M2M max. separation distance ($d_{j,j}$)	20 m
Transmission power of CUE ($P^c_{i,z}$)	100 mW
Transmission power of M2M (P^m_j)	17.23 dBm
Total transmission power of eNodeB (P_T)	2 W
SINR of CUs (ϑ^c_i)	20 dB
SINR of M2Ms (ϑ^m_j)	[− 15 dB, 15 dB]

SINR between the pre-fault and post-optimisation, for example, differed by 32dB for a 10-device count and decreased by 12.9 dB for a 50-device count.

The MOPSO algorithm balances SINR and throughput by adjusting bandwidth, transmit power, and device spacing. Device placement, power levels, and bandwidth were all adjusted using a dynamic optimisation technique. The optimal setup for ten devices needed 500 m between devices, 80 MHz bandwidth, and 22.0 dBm of transmission power. Wider bandwidths and higher transmission power levels were employed by the system to sustain performance as the number of devices increased. These model parameters change as a result of the particular operating compromises needed for massive systems, as shown in Table 9. With a disproportionate rise in the number of devices, the network experiences higher levels of congestion, interference, and communication stress, necessitating effective resource allocation to maintain performance. When the number of devices increases to 20 and beyond, the maximum bandwidth of 100 MHz is often used, indicating the need for more spectrum to avoid congestion and maintain the signal-to-interference-plus-noise ratio (SINR). Multi-objective particle swarm optimisation (MOPSO) appears to have found a better trade-off between bandwidth utilisation and other aspects, Such as power and spacing, likely due to interference dynamics, as the bandwidth drops to 73MHz when the number of devices approaches 30. This magnitude of bandwidth consumption must have been mostly caused by the growth in device density, but MOPSO strategically trades off bandwidth allocation against other constraints, so this does not occur linearly.

Additionally, as transmit (Tx) power influences signal strength, interference, and energy efficiency, the MOPSO algorithm maximises power when required while restricting it to prevent needless interference or energy waste. With up to 30 devices, power levels stay low (between 21.9 and 23.5 dBm), but at 40 devices, they rise to 27.9 dBm, Suggesting that more power is needed to combat interference and preserve link quality. Power drops marginally to 25.7 dBm at 50 devices, most likely as a result of optimised subgrouping and spacing that helps offset high density. Because M2M devices are separated by a large distance (500 m) and a small number of devices (10), there is less interference. The distance between devices decreases to roughly 424.7 m when there are 30 devices, which improves resource utilisation

Table 4 IEEE 9-bus system parameters for pre-fault system condition

	Number		*P* (MW)	*Q* (MVar)
Buses	9	Total generation capacity	820.0	− 900.0 to 900.0
Generators	3	On-line capacity	820.0	− 900.0 to 900.0
Committed gens	3	Generation (actual)	319.6	22.8
Loads	3	Load	315.0	115.0
Fixed	3	Fixed	315.0	115.0
Dispatchable	0	Dispatched	− 0.0 of 0.0	− 0.0
Shunts	0	Shunt (inj)	− 0.0	0.0
Branches	9	Losses (I^2 *Z)	4.64	48.38
Transformers	0	Branch charging (inj)	-	140.5
Inter-ties	0	Total inter-tie flow	0.0	0.0
Areas	1			

Table 5 IEEE 9-bus key power flow operating system parameters for pre-fault condition

	Minimum	Maximum
Voltage magnitude	0.996 p.u. @ bus 9	1.040 p.u. @ bus 1
Voltage angle	-3.99^0 @ bus 9	9.28° @ bus 2
P losses ($I^{2*}R$)	-	2.30 MW @ line 8–9
P losses ($I^{2*}X$)	-	15.83 MVar @ line 8–2

while limiting the detrimental effects of interference. At 40 and 50 devices (about 495 to 500 m), the spacing increases once more, suggesting that further separation is required to reduce co-channel interference at very high densities. MOPSO optimises the spatial distribution to dynamically balance interference and coverage.

The clustering reflects the number of devices organised into communication subgroups. This makes it possible for scattered processing and localised communication, which

Table 6 IEEE 9-bus pre-fault bus data system condition

Bus #	Voltage		Generation		Load	
	Mag (p.u.)	Ang (deg)	P (MW)	Q (MVar)	P (MW)	Q (MVar)
1	1.040	0.000*	71.64	27.05	-	-
2	1.025	9.280	163.00	6.65	-	-
3	1.025	4.665	85.00	−10.86	-	-
4	1.026	−2.217	-	-	-	-
5	1.013	−3.687	-	-	90.00	30.00
6	1.032	1.967	-	-	-	-
7	1.016	0.728	-	-	100.00	35.00
8	1.026	3.720	-	-	-	-
9	0.996	−3.989	-	-	125.00	50.00
Total			319.64	22.84	315.00	115.00

Table 7 IEEE 9-bus pre-fault system condition for branch data

Branch #	From bus	To bus	From bus injection		To bus injection		Loss ($I^{2*}Z$)	
			P (MW)	Q (Mvar)	P (MW)	Q (Mvar)	P (MW)	Q (Mvar)
1	1	4	71.64	27.05	−71.64	−23.92	0.000	3.12
2	4	5	30.70	1.03	−30.54	−16.64	0.166	0.90
3	5	6	−59.46	−13.46	60.82	−18.07	1.354	5.90
4	3	6	85.00	−10.86	−85.00	14.96	0.000	4.10
5	6	7	24.18	3.12	−24.10	−24.30	0.088	0.75
6	7	8	−75.90	−10.70	76.38	−0.80	0.475	4.03
7	8	2	−163.00	9.18	163.00	6.65	0.000	15.83
8	8	9	86.62	−8.38	−84.32	−11.31	2.300	11.57
9	9	4	−40.68	−38.69	40.94	22.89	0.258	2.19
Total						4.641	48.38	

Table 8 Performance metrics comparison across device counts for IEEE 9-bus smart grid system

Device count	Delay (s) (pre → post)	Opt clearance (s)	SINR dB (pre → post)	Throughput Mbps (pre → post)	Bandwidth MHz	Transmit power (dBm)	Distance (m)	Improvement (%)
10	0.066 → 0.053	0.166 → 0.153	37.0 → 69.4	860.46 → 1287.4	80	22.0	500.0	19.2
20	0.064 → 0.056	0.164 → 0.156	39.8 → 55.1	925.73 → 1282.0	100	23.5	460.0	11.5
30	0.070 → 0.057	0.170 → 0.157	32.6 → 52.7	759.08 → 893.0	73	21.9	425.0	17.8
40	0.071 → 0.060	0.171 → 0.160	30.9 → 45.9	717.76 → 1067.98	100	27.9	496.0	15.9
50	0.070 → 0.061	0.170 → 0.161	32.1 → 45.0	747.30 → 1046.65	100	25.7	500.0	13.6

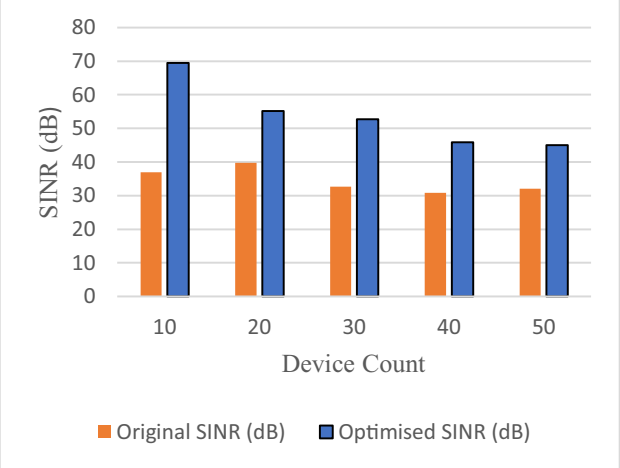

Fig. 3 Original and optimised SINR (dB) enhancement comparison against device count

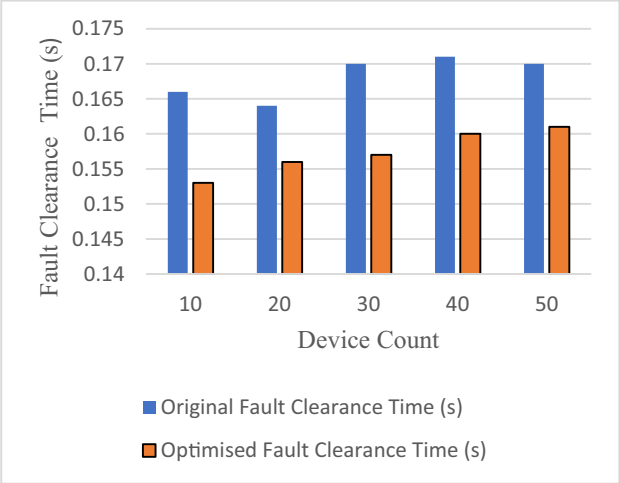

Fig. 5 Pre-optimised and optimised fault clearance time (s) comparison against device count

enhances scalability and reduces traffic congestion. As the number of devices increases, it scales linearly (5 for 10 devices, 25 for 50 devices). The network may efficiently expand from 10 to 50 devices while maintaining optimal operating conditions by using hierarchical clustering to manage device density and maintain efficient bandwidth and power usage. By regulating bandwidth, power, and spacing, the integrated MOPSO effectively controls interference, SINR, and throughput. As the number of devices increases, the system adapts by clustering and spacing devices to avoid performance degradation. The results in Table 8 demonstrate that the algorithm consistently finds optimal or nearly optimal configurations to achieve optimal convergence of resources under a range of conditions.

Key metrics like power loss and active and reactive power flows across branches 1 through 9 are represented in Fig. 7 under three distinct system conditions: pre-fault (blue bars represent normal operation), during fault (orange bars represent fault state), and post-optimisation (yellow bars represent MOPSO optimisation). These simulations are used to assess the algorithm's effect on grid stability. Most branches show consistent positive/negative flows before the fault under normal load levels, indicating a balanced bidirectional power exchange. Particularly, branches 1, 5, and 8 have substantial

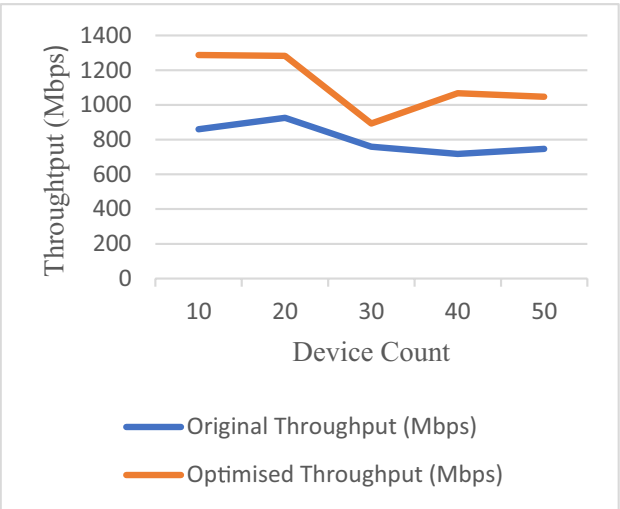

Fig. 4 Throughput improvement trend against changes in device count

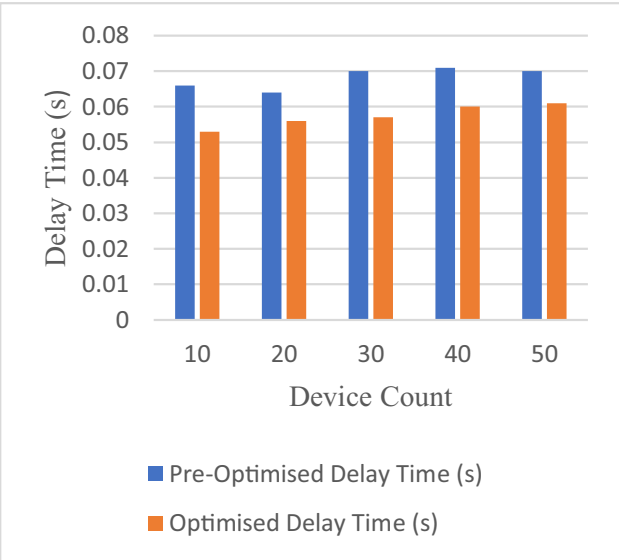

Fig. 6 Pre-optimised and optimised communication delay time (s) comparison against device count

Table 9 Optimal parameters for each scenario

Device count	Optimal bandwidth (MHz)	Optimal Tx power (dBm)	Optimal spacing (m)	Subgroup size
10	80	22.0	500.0	5
20	100	23.5	460.2	10
30	73	21.9	424.7	15
40	100	27.9	495.6	20
50	100	25.7	500.0	25

Table 10 Smart grid power flow analysis

Condition	Total real power loss (MW)	Min voltage (p.u.)	Max voltage (p.u.)	Avg voltage (p.u.)
Pre-fault	4.64	0.996	1.040	1.022
During-fault	4.97	1.001	1.049	1.029
Post-optimisation	4.69–4.73	0.995	1.040	1.022

magnitudes, demonstrating their crucial role in load support. Additionally, modelling results demonstrated that during fault conditions, power flow significantly decreased across several branches (e.g., 1, 2, 3, 6, and 7). As branches 4 and 6 change their direction and branch 7 gets closer to − 180 MW, it is clear that the disturbance propagation effect is to blame for this decline. This effect denotes system instability brought on by higher losses or flow obstructions from relay action or fault isolation. Additionally, the simulation findings show that the power flow magnitudes, particularly on branches 1, 3, 6, and 8, are more balanced and enhanced, nearly exactly duplicating the pre-fault values. Nevertheless, there is still a sizable negative flow in branch 7, which is now constant and most likely reassigned through efficient load sharing. The technical ramifications demonstrated that although faults severely impair power delivery, the use of MOPSO optimisation aids in power flow redistribution and restoration, enhancing grid resilience and supply continuity and lowering overload or underload across branches.

To preserve voltage stability, the pre-fault state showed a moderate reactive power demand (positive and negative flows) for the Reactive Power Flow (MVAR). Branches 1 and 7, which show voltage control, contribute the most, but during fault situations, reactive power drastically drops or reverses, particularly in branches 4 and 9. For instance, branch 9 approaches −50 MVAR when negative readings

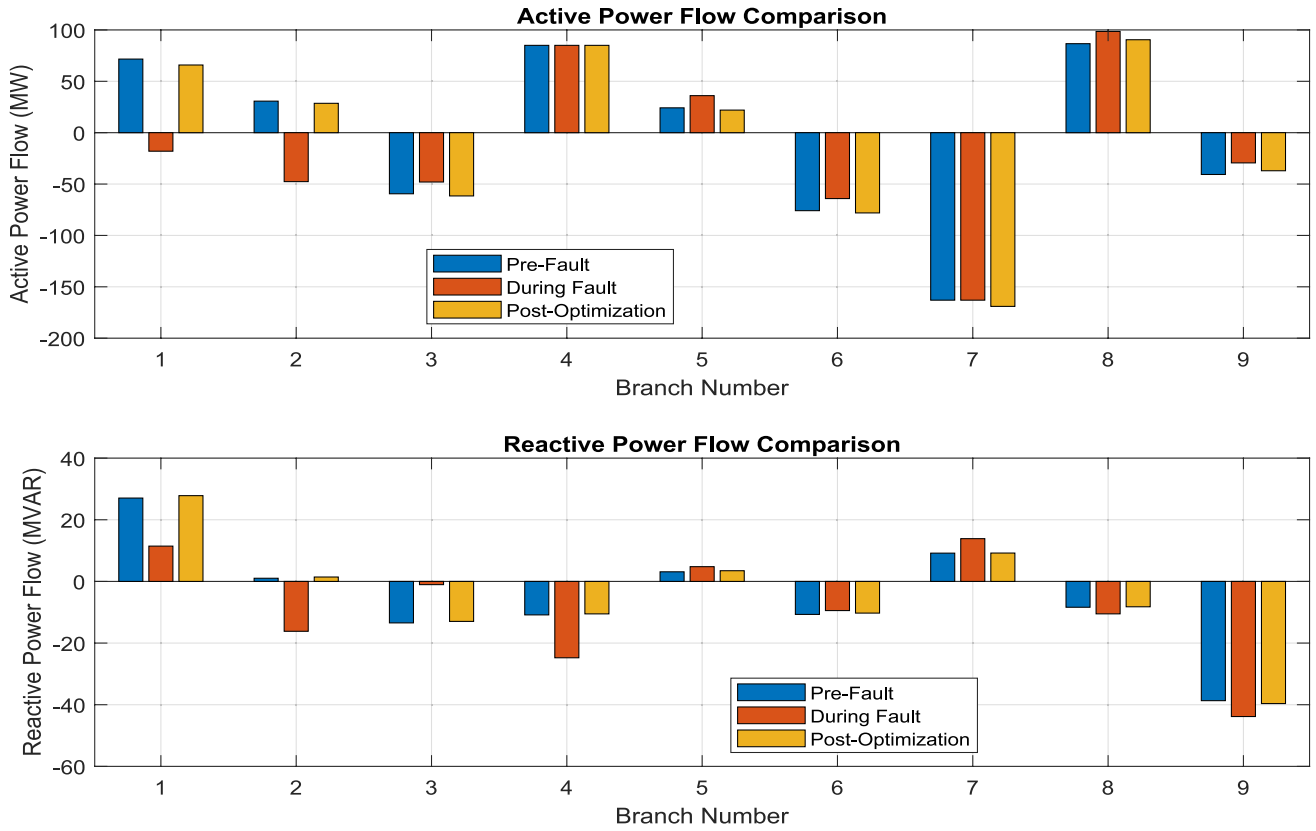

Fig. 7 Comparison of the reactive and active power flow analysis across transmission branches in a smart grid network under pre-fault, during fault, and post-optimisation conditions

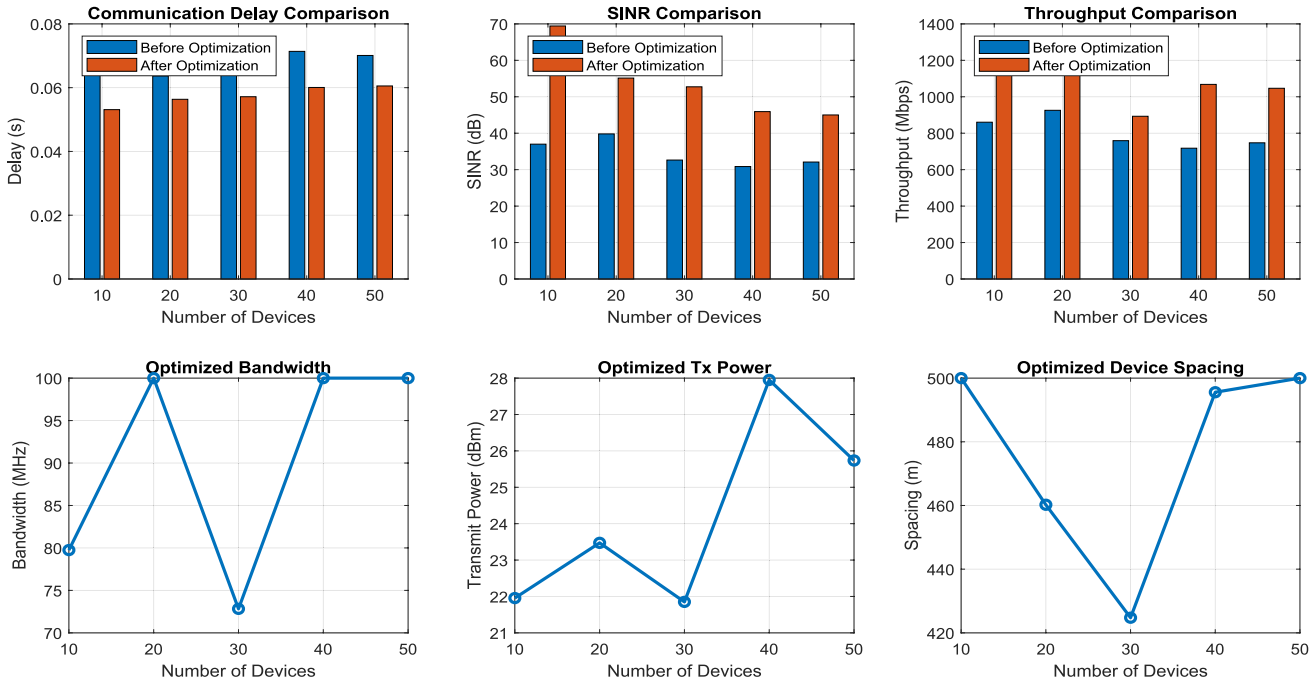

Fig. 8 Performance metrics comparison for communication delay, SINR, and throughput for pre-optimisation and post-optimisation conditions

spike, suggesting a considerable lagging load or the possibility of voltage collapse during a fault or interference. As a result, most branches (especially 1, 4, 7, and 9) showed improved reactive flow during the Post-Optimisation condition. Values that are more stable and closer to pre-fault levels guarantee better power factor control and voltage profile recovery. However, the post-optimisation results from the addition of MOPSO showed improvements in voltage stability by preventing voltage sags or swells and aiding reactive compensation. Technically, this implies that the reactive power behaviour exhibits instability during a fault, especially in load-sensitive branches.

The resilience and stability of the system are shown in Table 10, which is based on observations of the different changes in voltage and power loss under different conditions. With a 4.64 MW total actual power loss and voltage levels within a regulated range (0.996–1.040 p.u., with an average of 1.022 p.u.), the system operates normally during the pre-fault condition, Suggesting a steady-state condition. But in the fault scenario, the real power loss rises to 4.97 MW, indicating increased system stress. As illustrated in Fig. 8, slight fluctuations in voltage levels (1.001–1.049 p.u., with an average of 1.029 p.u.) were noted, suggesting that the fault disrupts the smart grid network but does not lead to significant instability. The total real power loss is still more than it was before the pre-fault state, even though the post-optimisation condition and integration of the MOPSO technique, which were intended to minimise the impact of the fault, slightly reduced the power loss (4.89–4.93 MW). The voltage regulation's stability (0.995–1.040 p.u., with an average of 1.022 p.u.) indicates that the system's stability has been aided by optimisation. On the other hand, higher real power loss during a fault is an indication of systemic disruption resulting in an induced energy inefficiency, and such faulty voltage fluctuations could be controlled to avoid significant operational disruptions. Optimisation may result in a slight decrease in power loss, but the system does not fully return to its pre-fault state. This highlights the need for ongoing stability enhancements.

In a smart grid network with 10–50 connected devices, Fig. 8 provides a detailed comparison of communication performance measures and the values of their optimised parameters. The outcomes of optimisation, both before and after applying the multi-objective particle swarm optimisation (MOPSO) technique, are included in this. According to the simulation results, the MOPSO algorithm's application resulted in a considerable reduction in communication delay across the board. This delay reduction demonstrates how the MOPSO's integration and implementation can improve MTDs' real-time responsiveness, particularly when used in smart grid applications with low latency. Additionally, after the MTDs were optimised using the developed MOPSO method, the SINR values grew slowly and consistently, with devices achieving SINR increases of up to 30 dB. This enhancement implies that only reduced packet loss and retransmission under certain interference scenarios are

Table 11 Performance evaluation of MOPSO algorithm benchmarked against NSGA-II (MOGA) using IEEE 9-bus smart grid system

Device count	Pre-optimisation SINR (dB)	MOPSO optimisation SINR (dB)	NSGA-II optimisation SINR (dB)
100	29.24	41.28	44.25
200	25.06	36.03	43.56
300	22.26	39.03	34.65
400	21.25	46.82	26.70
500	19.77	29.36	34.59
	Pre-optimisation delay (ms)	MOPSO-optimisation delay (ms)	NSGA-II optimisation delay (s)
100	73.10	62.69	60.94
200	78.56	66.50	61.32
300	82.86	64.20	67.68
400	84.56	59.62	76.31
500	87.20	73.03	67.73
	Pre-optimisation fault clearance time (ms)	MOPSO optimisation fault clearance time (ms)	NSGA-II optimisation fault clearance time (ms)
100	173.16	162.69	160.94
200	178.56	166.50	161.32
300	182.86	164.20	167.68
400	184.56	159.62	176.31
500	187.20	173.03	167.73
	Pre-optimisation throughput (Mbps)	MOPSO optimisation throughput (Mbps)	NSGA-II optimisation throughput (Mbps)
100	658.06	722.23	885.13
200	569.22	1017.82	445.87
300	522.44	762.00	1068.87
400	482.12	371.59	849.73
500	473.17	838.35	689.21
		MOPSO bandwidth (MHz)	NSGA-II bandwidth (MHz)
100		100	91.55
200		91.54	98.12
300		35.41	93.47
400		20	92.46
500		100	56.80
		MOPSO Tx power (dBm)	NSGA-II Tx power (dBm)
100		18.16	26.47
200		10	10.46
300		10	19.48
400		26.58	22.25
500		30	22.72
		MOPSO spacing (*m*)	NSGA-II spacing (*m*)
100		410.41	301.47
200		205.35	377.95
300		275.46	165.92
400		461.15	85.83
500		116.52	244.07

assured in a densely populated heterogeneous M2M environment with strong communication links.

Furthermore, during the post-optimisation condition, the system throughput showed a notable improvement across all device counts, demonstrating MOPSO's effective bandwidth utilisation capability. The system is scalable because of this increase in throughput, which guarantees that the network can handle significant data traffic from multiple other MTDs, including faulty motors, controllers, wireless sensors, and internet of things devices.

By increasing the bandwidth allocation, which peaks at a maximum of 100 MHz for device counts of 20, 40, and 50,

Table 12 Comparative analysis of the performance of the MOPSO and NSGA-II optimisation algorithm

Metric	Pre-optimisation	MOPSO	NSGA-II
SINR	Low SINR across all device counts due to unmanaged interference	Consistently improves SINR; especially strong under high device density; stable across scenarios	High SINR at low device counts, but unstable at higher loads; performance drops with increasing devices
Fault clearance time	Long clearance times with increasing device count	Consistently reduces clearance time across all device counts; reliable under heavy load	Slightly better than MOPSO under small loads, but degrades with higher device counts
Delay	High delays are increasing with device count	Maintains relatively low and stable delays; scalable for large networks	Very low delay at low device counts, but less stable at higher loads
Bandwidth allocation	Static allocation; inefficient under interference	Aggressive adaptation with extreme allocations (min or max) to mitigate interference	More evenly distributed allocation, but less adaptive under interference
Throughput	Generally low throughput with device scaling	Balanced throughput across device counts while avoiding sharp fluctuations	Achieves peak throughput under moderate loads but is unstable; large performance swings occur at different loads
Transmit power	Fixed values, not optimised	Flexible allocation; adjusts widely (low to high) depending on network state	Moderate, less variable allocation; prioritises efficiency over adaptability
Spacing	Random or fixed spacing; interference not managed	Larger spacing under higher loads to reduce collisions and interference	Allows tighter clustering to increase capacity, but risks higher interference

respectively, the network's congestion avoidance and frequency reuse factor improved proportionately as the number of devices increased. Additionally, the MOPSO algorithm changed the MTDs' transmit power in a nonlinear way. The increased distance spacing of the MTDs or the dense attributes within the network are responsible for the peaked power allocation of 27.9 dBm at 40 devices. This necessitates the allocation of more power within the devices' coverage area to compensate for both intra- and inter-interferences while maintaining a high SINR.

Additionally, the optimal separation distance between devices showed a uniform decrease at 30 devices, and then increased again as the device count increased between 40 and 50. The technical implication is that the closer separation distance at moderate device counts is advantageous because the system allocates less power to MTDs, while the increased separation distance mitigates the consequences of co-channel interference. This feature of the MOPSO is strategic in balancing the trade-off between communication range and interference control.

The performance characteristics of the MOPSO and NSGA-II for the IEEE 9-bus smart grid network are compared in Table 11. The data given compares pre-optimisation, MOPSO optimisation, and NSGA-II optimisation across several key performance characteristics for 5G M2M communication, with device counts ranging from 100 to 500. The pre-optimisation SINR is low, indicating high interference and poor signal clarity, according to an analysis of the signal-to-interference-plus-noise ratio (SINR). When there are fewer devices (up to 44.25 dB for 100 devices), the SINR rises with the MOPSO algorithm for all device counts, reaching a high of 46.82 dB for 400 devices. However, as Fig. 8 illustrates, NSGA-II works better when there are more than 300 devices, yet the SINR drops to 26.70 dB for 400 devices. MOPSO provides better stability for large device counts, whereas NSGA-II favours lower device densities for SINR increase. As a result, SINR is an essential metric for wireless communications signal quality. However, both optimisation algorithms reduce delay; however, MOPSO consistently delivers lower latency with higher device counts. The NSGA-II increases the latency to 76.31 ms for 400 devices in comparison to MOPSO, indicating possible optimisation congestion issues in the smart grid network. Because MOPSO continuously lowers latency, it becomes more reliable and appropriate for real-time applications like smart grid applications, as shown in Table 12.

MOPSO achieves quicker fault clearance intervals, which increases the network's resilience to failures. Although NSGA-II performs better for smaller device counts, MOPSO achieved a fault clearance time of 159.62 ms for 400 devices, whereas NSGA-II increased the fault clearance time to 176.31 ms for the same number of devices. The results of the deductions demonstrated that MOPSO provides more dependable error recovery, which is necessary for critical M2M applications. According to the system throughput performance, MOPSO performs better with fewer devices and peaks at 959.93 Mbps for 100 devices. However, for 200 devices, NSGA-II outperforms MOPSO in terms of throughput value, achieving 993.87 Mbps. MOPSO's throughput drops after 300 devices, peaking at a lower 217.75 Mbps for 400 devices. The simulation results in Table 12 demonstrated that

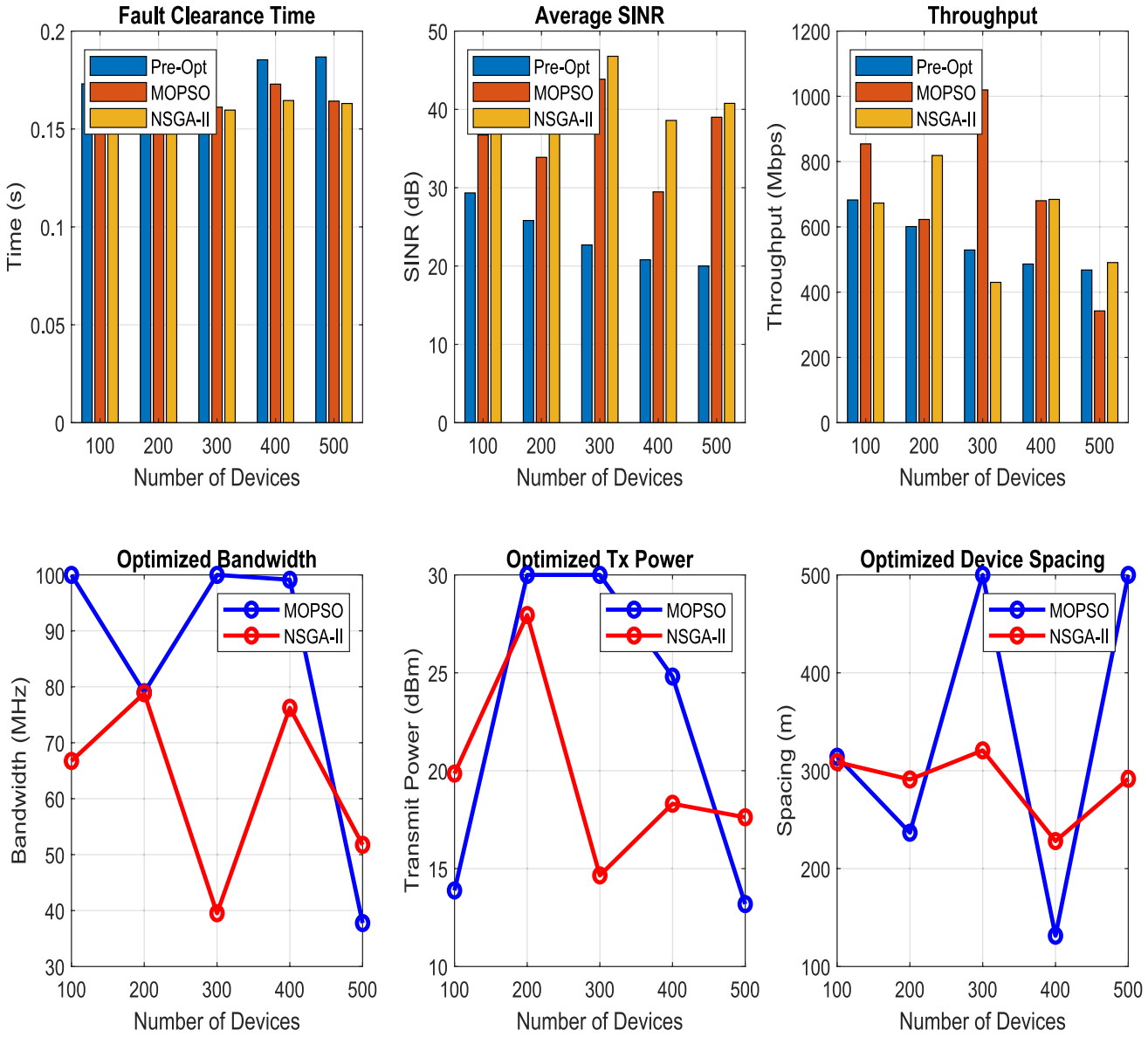

Fig. 9 Comparison of performance metrics between *f*ault clearance time (s), *a*verage SINR (dB), and *t*hroughput (Mbps) for *p*re-*o*ptimisation *c*ondition, MOPSO, and NSGA-II *a*lgorithms

MOPSO provides fault recovery stability for all device densities. As seen in Fig. 9, NSGA-II is more effective in maximising throughput. Important numerical data demonstrates that MOPSO consistently sustains higher bandwidth allocation (100 MHz for 100 and 500 devices). However, the NSGA-II Suggests a reduced bandwidth allocation for 500 devices (56.80 MHz) to maximise power efficiency. The algorithm's transmit power in NSGA-II was higher (26.47 dBm) than in MOPSO (18.16 dBm) when 100 devices were used. Furthermore, the spacing varies significantly; NSGA-II maintains modest distances (85.83 m for 400 devices), while MOPSO displayed a broad spacing (461.15 m for 400 devices) to minimise the influence of interference.

5 Conclusion

In this paper, the interference problem was investigated in machine-to-machine (M2M) communications underlaying 5G cellular networks. The interference problem, when applied within the smart grid (SG), results in a combinatorial and non-convex optimisation with a multi-dimensional matching problem, which is known to be non-deterministic

polynomial (NP)-hard. To resolve the optimisation problem, the MOPSO algorithm was developed to simultaneously maximise both the throughput and SINR within the communication domain, and minimise the power loss, fault clearance time, and communication delay time within the smart grid power domain. However, simulation of the various interference (fault) conditions (pre-fault, during-fault, and post-optimisation) showed that the integration of MOPSO enhanced the throughput and SINR in the post-optimisation condition when compared with the pre-fault state and During-fault condition within the communication domain. Similarly, the post-optimisation integration of MOPSO within the SG domain decreased IEEE 9-bus power loss close to the pre-fault state, and also decreased the communication delay and the fault clearance time relative to the pre-fault and during-fault conditions. The performance of the MOPSO algorithm was compared with NSGA-II, and simulation results showed that MOPSO outperformed the benchmarked algorithm in terms of average SINR, throughput, and fault clearance time. Furthermore, the results also proved that MOPSO depicts a uniform and consistent pattern in optimising the bandwidth, power, and placement distance. The influence of interference on M2M communication within a smart grid power system has been studied, and the implementation of the developed MOPSO algorithm has enhanced both the communication between MTDs and improved the fault clearance time, showing swift network recovery and resilience.

Acknowledgements The authors wish to thank The Federal Polytechnic, Ilaro for their support and opportunity in conducting this research work.

Author contribution Suleiman, Ahmed Danasabe contributed to the system modelling, theoretical analysis, algorithm design, and writing of this article. Ibrahim Abdullahi also contributed to system modelling and optimisation. Mohammed Abubakar Saddiq, Salihu Bala Alhaji, David Micheal, and Micheal Ephraim supervised the work and proofread this article. The authors read and approved the final manuscript.

Funding The authors did not receive any support from any organisation for the submitted work.

Data availability There are no data available for this study.

Declarations

Competing interests The authors declare no competing interests.

References

Abdulkareem A, Somefun TE, Awosope COA, Olabenjo O (2021) Power system analysis and integration of the proposed Nigerian 750-kV power line to the grid reliability. SN Appl Sci. https://doi.org/10.1007/s42452-021-04847-3

Abdulsalam, K. A., Adebisi, J., Emezirinwune, M., & Babatunde, O. (2023). An overview and multicriteria analysis of communication technologies for smart grid applications. *E-Prime - Advances in Electrical Engineering, Electronics and Energy*, *3*(December 2022), 100121. https://doi.org/10.1016/j.prime.2023.100121

Achaal B, Adda M, Berger M, Ibrahim H, Awde A (2024) Study of smart grid cyber-security, examining architectures, communication networks, cyber-attacks, countermeasure techniques, and challenges. Cybersecurity 7(1):10. https://doi.org/10.1186/s42400-023-00200-w

Ahsan F, Dana NH, Sarker SK, Li L, Muyeen SM, Ali MF, Tasneem Z, Hasan MM, Abhi SH, Islam MR, Ahamed MH, Islam MM, Das SK, Badal MFR, Das P (2023) Data-driven next-generation smart grid towards sustainable energy evolution: techniques and technology review. Prot Control Mod Power Syst 8(1):43. https://doi.org/10.1186/s41601-023-00319-5

Alam MJ, Chugh R, Azad S, Hossain R (2024) Ant colony optimization - based solution to optimize load balancing and throughput for 5G and beyond heterogeneous networks. EURASIP J Wirel Commun Netw. https://doi.org/10.1186/s13638-024-02376-2

AlSheyab HY, Choudhury S, Bedeer E, Ikki SS (2020) Interference minimization algorithms for fifth-generation and beyond systems. Comput Commun 156(2020):145–158. https://doi.org/10.1016/j.comcom.2020.03.046

Antonius Alijoyo, F., Vidhate, D. A., Kaur, C., Nivedan, V., Rani, V. K., & Balakumar, A. (2024). Cloud-based IoT solutions for smart grids: advancing smart technologies in energy management. *2024 IEEE 3rd International Conference on Electrical Power and Energy Systems (ICEPES)*, *December*, 1–6. https://doi.org/10.1109/ICEPES60647.2024.10653566

Barman, K., & Ajay, R. (2020). A combine mode selection based resource allocation and interference control technique for D2D communication. *2020 7th International Conference on Signal Processing and Integrated Networks (SPIN)*, 284–289. https://doi.org/10.1109/SPIN48934.2020.907096

Cheng S, Liu J, Wang L (2021) Controlling interference structure and transmit power of aerial small cells by hybrid affinity propagation clustering and reinforcement learning. IEEE Open J Veh Technol 2:412–418. https://doi.org/10.1109/OJVT.2021.3112468

Das SK, Hossain MF (2020) A location-aware power control mechanism for interference mitigation in M2M communications over cellular networks. Comput Electr Eng 88:106867. https://doi.org/10.1016/j.compeleceng.2020.106867

Dubey R, Mishra PK, Pandey S (2020) Mixed uplink, downlink channel allocation and power allocation schemes for 5G networks. Wirel Pers Commun 112(4):2253–2274. https://doi.org/10.1007/s11277-020-07148-x

Elrawy MF, Tekki E, Hadjidemetriou L, Laoudias C, Michael MK (2023) Protection and communication model of intelligent electronic devices to investigate security threats. IEEE Power & Energy Society Innovative Smart Grid Technologies Conference (ISGT) 2023:1–5. https://doi.org/10.1109/ISGT51731.2023.10066371

Gaspar J, Cruz T, Lam C-T, Simões P (2023) Smart substation communications and cybersecurity: a comprehensive survey. IEEE

Commun Surv Tutor 25(4):2456–2493. https://doi.org/10.1109/COMST.2023.3305468

Hao B, Lv B, Chen Q, Li X (2023) A two-stage real-time optimization model of arterial signal coordination based on reverse causal-effect modeling approach. Sustainability 15(18):14035. https://doi.org/10.3390/su151814035

Hassan N, Fernando X (2019) Interference mitigation and dynamic user association for load balancing in heterogeneous networks. IEEE Trans Veh Technol 68(8):7578–7592. https://doi.org/10.1109/TVT.2019.2919812

Hu S, Chen X, Ni W, Wang X, Hossain E (2020) Modeling and analysis of energy harvesting and smart grid-powered wireless communication networks: a contemporary survey. IEEE Trans Green Commun Netw 4(2):461–496. https://doi.org/10.1109/TGCN.2020.2988270

Kabeyi MJB, Olanrewaju OA (2023) Smart grid technologies and application in the sustainable energy transition: a review. Int J Sustain Energy 42(1):685–758. https://doi.org/10.1080/14786451.2023.2222298

Kaufman B, Lilleberg J, Aazhang B (2013) Spectrum sharing scheme between cellular users and ad-hoc device-to-device users. IEEE Trans Wireless Commun 12(3):1038–1049. https://doi.org/10.1109/TWC.2012.011513.120063

Kumar, S., Mishra, K. V., Gautam, S., M. R., B. S., & Ottersten, B. (2021). Interference mitigation methods for coexistence of radar and communication. *2021 15th European Conference on Antennas and Propagation (EuCAP)*, 1–4. https://doi.org/10.23919/EuCAP51087.2021.9411250

Labrador Rivas AE, Abrão T (2020) Faults in smart grid systems: monitoring, detection and classification. Electr Power Syst Res 189(May):106602. https://doi.org/10.1016/j.epsr.2020.106602

Liu X, Xiao H, Chronopoulos AT (2020) Joint mode selection and power control for interference management in D2D-enabled heterogeneous cellular networks. IEEE Trans Veh Technol 69(9):9707–9719. https://doi.org/10.1109/TVT.2020.3001874

Majeed Butt O, Zulqarnain M, Majeed Butt T (2021) Recent advancement in smart grid technology: future prospects in the electrical power network. Ain Shams Eng J 12(1):687–695. https://doi.org/10.1016/j.asej.2020.05.004

Nguyen VH, Abil H, Herrera DR, Thomas R, Coste T (2025) Containerized IEC 61850-based protection in smart grid – lab demonstration and performance assessment for large scale deployment. Electr Power Syst Res 249:111999. https://doi.org/10.1016/j.epsr.2025.111999

Osama M, El Ramly S, Abdelhamid B (2021) Interference mitigation and power minimization in 5G heterogeneous networks. Electronics 10(14):1723. https://doi.org/10.3390/electronics10141723

Pandey K, Arya R (2022) Lyapunov optimization machine learning resource allocation approach for uplink underlaid D2D communication in 5G. IET Commun 16:476–484. https://doi.org/10.1049/cmu2.12264

Patel, D. K., Phukan, H., Mansani, S., Singh, J., Sreejith, S., Goswami, A. K., & Patel, R. (2023). Smart grid communication and information technologies: a review. In *Lecture Notes in Networks and Systems* (Vol. 443, Issue June 2023, pp. 45–59). https://doi.org/10.1007/978-981-19-2764-5_5

Pourkabirian A, Anisi MH, Kooshki F (2021) A game-based power optimization for 5G femtocell networks. Comput Commun 177(July):230–238. https://doi.org/10.1016/j.comcom.2021.07.022

Raza N, Akbar MQ, Soofi AA, Akbar S (2019) Study of smart grid communication network architectures and technologies. J Comput Commun 07(03):19–29. https://doi.org/10.4236/jcc.2019.73003

Saini, M., Khan, S., Singh, S., Gupta, R., Upadhyay, P., & Soni, S. (2021). Smart grid: problems, Avenues for Study & Attainable Solutions. *2021 International Conference on Advance Computing and Innovative Technologies in Engineering (ICACITE)*, *7*, 513–518. https://doi.org/10.1109/ICACITE51222.2021.9404566

Shafiei A, Jamshidi M, Khani F, Talla J, Peroutka Z, Gantassi R, Baz M, Cheikhrouhou O, Hamam H (2021) A hybrid technique based on a genetic algorithm for fuzzy multiobjective problems in 5G, Internet of Things, and mobile edge computing. Math Probl Eng. https://doi.org/10.1155/2021/9194578

Shahinzadeh, H., Mahmoudi, A., Moradi, J., Nafisi, H., Kabalci, E., & Benbouzid, M. (2021). Anomaly detection and resilience-oriented countermeasures against cyberattacks in smart grids. *2021 7th International Conference on Signal Processing and Intelligent Systems (ICSPIS)*, *December*, 1–7. https://doi.org/10.1109/ICSPIS54653.2021.9729386

Song X, Wang K, Lei L, Zhao L, Li Y, Wang J (2020) Interference minimization resource allocation for V2X communication underlaying 5G cellular networks. Wirel Commun Mob Comput 2020:1–9. https://doi.org/10.1155/2020/2985367

Su W, Mu C, Xue L, Yang X, Zhu S (2025) An improved traffic coordination control integrating traffic flow prediction and optimization. Eng Appl Artif Intell 143:109969. https://doi.org/10.1016/j.engappai.2024.109969

Suleiman, A. D., Mohammed, A. S., Salihu, B. A., & David, M. (2022). Resource allocation and management in Machine-to-Machine (M2M) communication in underlay in-band cellular network: a survey. *4th International Engineering Conference (IEC 2022)*, *17*, 428–434. futminna.edu.ng%0AResource Allocation and Management in Machine-to-Machine (M2M)

Suleiman, A. D., Abubakar Sadiq, M., Bala Alhaji, S., David, M., Abdullahi, I., & Micheal, E. (2024). Proposed architecture and mathematical model to enhance interference management in 5G-enabled M2M networks. *International Journal of Innovation in Engineering*, *5*(1), 24–41. https://doi.org/10.59615/ijie.5.1.24

Ullah MH, Eskandarpour R, Zheng H, Khodaei A (2022) Quantum computing for smart grid applications. IET Gener Transm Distrib 16(21):4239–4257. https://doi.org/10.1049/gtd2.12602

Velasquez W, Moreira-Moreira GZ, Alvarez-Alvarado MS (2024) Smart grids empowered by software-defined network: a comprehensive review of advancements and challenges. IEEE Access 12(April):63400–63416. https://doi.org/10.1109/ACCESS.2024.3396402

Wang, X., Fei, Z., Huang, J., Zhang, J. A., & Yuan, J. (2021). Joint resource allocation and power control for radar interference mitigation in multi-UAV networks. *Science China Information Sciences*, *64*(182307:2), 1–13. https://doi.org/10.1007/s11432-020-3133-x

Wang X, Fidge C, Nourbakhsh G, Foo E, Jadidi Z, Li C (2022) Anomaly detection for insider attacks from untrusted intelligent electronic devices in substation automation systems. IEEE Access 10:6629–6649. https://doi.org/10.1109/ACCESS.2022.3142022

Yamashita K, Yang Z, Ten C, Kar S, Ginter A (2022) Cascading verification initiated by switching attacks through compromised digital relays. IET Smart Grid 5(3):189–202. https://doi.org/10.1049/stg2.12062

Yasin Ghadi Y, Mazhar T, Aurangzeb K, Haq I, Shahzad T, Ali Laghari A, Shahid Anwar M (2024) Security risk models against attacks in smart grid using big data and artificial intelligence. PeerJ Comput Sci 10:e1840. https://doi.org/10.7717/peerj-cs.1840

Yuan, D., Nam, Y., Feriani, A., Konar, A., Wu, D., Jang, S., Liu, X., & Dudek, G. (2023). Mixed-variable PSO with fairness on multi-objective field data replication in wireless networks. *ICC 2023 - IEEE International Conference on Communications*, *2023-May*, 3720–3725. https://doi.org/10.1109/ICC45041.2023.10279642

Authors and Affiliations

Ahmed Danasabe Suleiman[1] · Abubabakar Saddiq Mohammmed[2] · Bala Alhaji Salihu[2] · Michael David[2] · Abdullahi Ibrahim Mohammed[3] · Ephraim Michael[4]

✉ Ahmed Danasabe Suleiman
ahmed.suleiman@federalpolyilaro.edu.ng

[1] Department of Computer Engineering, Federal Polytechnic Ilaro, Ogun State, Abeokuta, Nigeria

[2] Department of Telecommunication Engineering, Federal University of Technology Minna, Niger State, Minna, Niger State, Nigeria

[3] Department of Computer Engineering, Federal University of Technology, Minna, Niger State, Nigeria

[4] Department of Research and Development, Aeronautics and Aerial Vehicle Development Institute, Zaria, Kaduna state, Nigeria